New criterion for direct black hole formation in rapidly rotating stellar collapse

Yu-ichirou Sekiguchi and Masaru Shibata

Graduate School of Arts and Sciences, University of Tokyo, Tokyo, 153-8902, Japan

(Received 8 March 2004; published 4 October 2004; publisher error corrected 12 October 2004)

We study gravitational collapse of rapidly rotating relativistic polytropes of adiabatic indices $\Gamma = 1.5$ and 2. The nondimensional spin parameter of the system $q \equiv J/M^2$ where J and M are the total angular momentum and the gravitational mass is set to be larger than unity. First, analyzing initial distributions of mass and spin parameters inside the stars, we predict the final outcome after the collapse proposing a new criterion for direct black hole formation as $q_c < 1$ where q_c denotes an effective spin parameter of the stellar central region. To confirm our predictions, we then perform fully general relativistic simulations assuming axial and equatorial symmetries. It is found that in contrast with previous conclusions for the criterion of no black hole formation, a black hole is formed even from a star with $q > 1$ if the condition $q_c < 1$ is satisfied. For $q_c < 1$, a seed black hole is always formed first, and then, it grows as the ambient fluid elements accrete onto it. We also find that the time evolution of the relation between angular momentum and mass enclosed in the seed black hole can be approximately determined from the initial profiles of the density and the specific angular momentum.

DOI: 10.1103/PhysRevD.70.084005 PACS numbers: 04.25.Dm, 04.30.–w, 04.40.Dg

I. INTRODUCTION

One of fundamental issues in numerical general relativity is to explore the final fate after gravitational collapse of rotating stellar cores. If their mass is much larger than the maximum mass of a neutron star $\sim 2M_\odot$, the collapse will proceed until a spacetime singularity is formed. If the cosmic censorship conjecture suggested by Penrose [1] is correct, any singularity should be surrounded by an event horizon. Then, the black hole uniqueness theorems of Israel [2], Carter [3], and Robinson [4] tell that the collapsed star will consequently settle down to a Kerr black hole.

It is well known that in a Kerr spacetime, the singularity is covered by an event horizon only if the nondimensional spin parameter defined as $q \equiv cJ/GM^2$, where J, M, c, and G are the total angular momentum, the gravitational mass, the speed of light, and the gravitational constant, does not exceed unity [5,6]. Otherwise the singularity is naked. This implies that the value of q of any black hole cannot be larger than unity. For realistic progenitors of black holes, however, the value of q may be larger than unity (e.g., [7]). Thus, it is interesting to explore the final fate after the gravitational collapse of rotating stars with $q > 1$. Numerical relativity is the unique approach to resolve this problem. In this paper, we explore this subject adopting a toy model from an gravitational-physical interest. Adopting appropriate toy models is often robust to extract a physical content clearly.

There have been several studies for gravitational collapse to a black hole in numerical relativity assuming axial symmetry [8–14]. A series of simulations for rotating stellar collapse in full general relativity was first performed by Nakamura [8] and his collaborators [9] using the $(2 + 1) + 1$ formalism developed by Maeda *et al.* [15]. They adopted *differentially rotating* massive stellar cores that are to collapse to a black hole. An interesting finding in their simulations is that q is a critical parameter for determining the prompt black hole formation. Their results suggest that for $q > 1$, no black hole is formed and the stars bounce back due to the centrifugal force, indicating that the cosmic censorship conjecture holds. Stark and Piran [10] subsequently performed simulations for the collapse of polytropes with *the adiabatic index* $\Gamma = 2$ and with an artificially given rigid rotation, using the Bardeen-Piran formalism [16]. They reconfirmed the conclusion suggested by Nakamura; for $q \gtrsim 1$, black hole is not formed. Abrahams *et al.* [11] studied the collapse of axisymmetric and *differentially rotating* tori composed of collisionless matter, and also found that black holes are formed only from initial configurations with $q \lesssim 1$. Shibata [13] studied the formation of black holes from marginally stable supramassive rotating polytropes at the mass-shedding limit with $\Gamma = 2.5, 2.25, 5/3$, and 1.5, for which $q < 1$, and found that the final state of such collapse is a Kerr black hole with no appreciable disk. Shibata and Shapiro [14] studied the collapse of a rigidly rotating polytrope at the mass-shedding limit with $\Gamma = 4/3$. The value of q for such a configuration is close to unity as ≈ 0.96 [17]. They found that the outcome is a black hole surrounded by an appreciable disk ($M_{\rm disk}/M \approx 0.1$).

There have been also preliminary three-dimensional simulations of the collapse of rotating neutron stars [18–21]. Shibata, Baumgarte, and Shapiro [18] performed simulations for collapse of marginally stable supramassive rotating polytropes at the mass-shedding limit with $\Gamma = 2$ and $q < 1$, and found that a black hole with no disk is the outcome. They also found no evidence for the nonaxisymmetric deformation. In [19–21], three-dimensional simulations were performed with the so-

called black hole excision technique [22]. In all the papers, the neutron stars were modeled by $\Gamma = 2$ relativistic polytropes and a preliminary black hole excision technique developed in [23] was adopted. Duez *et al.* [19] reconfirmed that for the collapse of the $\Gamma = 2$ polytrope, a black hole is formed only for the case $q < 1$. For $q > 1$, on the other hand, the collapsing star forms a torus of a nonaxisymmetric structure, in contrast with the result in the axisymmetric simulations. Baiotti *et al.* [20] also found that the final fate after the collapse of the neutron star rotating at the mass-shedding limit is a rotating Kerr black hole.

All these results suggest that the maximum value of q of a progenitor for the black hole formation is ~ 1, and that the final state after the gravitational collapse of rotating stars with $q < 1$ is a rotating Kerr black hole with a small disk mass.

However, the rotating stellar collapse in general relativity has not been studied in detail adopting *soft equations of state* which are realized in realistic stellar cores; e.g., iron stellar cores and pair-unstable oxygen cores for which the adiabatic indices $\Gamma < 4/3$ at the onset of the collapse. Recently, Shibata [7] determined marginally stable and rigidly rotating stars with soft equations of state ($\Gamma \lesssim 4/3$) against gravitational collapse, which are plausible initial conditions for rotating stellar core collapse. Based on the results of his stability analysis, he predicts that (i) even for a rigidly rotating star with $q > 1$, a central region, in which an approximate *local* value of q (denoted as q_c) is smaller than unity, will first collapse to form a black hole, if q is not too large ($q < 2.5$), and that (ii) as a result of the collapse for $q_c < 1$ and $q \gg 1$, a massive disk ($M_{\rm disk}/M = O(0.1)$) will be formed around the rotating black hole.

The physical basis of the above prediction can be explained as follows. Consider gravitational collapse of a rotating star with $q_c < 1$ and $q > 1$ in Newtonian gravity, and then focus on a central part of the star of mass M_0 and angular momentum J_0. In the absence of pressure, the gravitational attraction at the equatorial surface of the central part will eventually balance with the centrifugal force at a certain radius r_b in the Newtonian theory. Assuming that the mass and the angular momentum of the central part is conserved during the collapse, the balance radius is written as $r_b = J_0^2/(GM_0^3)$. For $q_0 \equiv cJ_0/(GM_0^2) < 1$, the radius satisfies $r_b < GM_0/c^2$, which indicates that the rotating fluid body would collapse to a black hole in general relativity. For $q_0 > 1$, on the other hand, the fluid body will bounce back due to the sufficiently strong centrifugal force. Therefore, a region of the rotating star in which a quasilocal value q_0 is less than unity may collapse to form a black hole. On the other hand, a region with $q_0 > 1$ may bounce back. The above simple consideration illustrates the importance of a quasilocal spin parameter (see Sec. III B).

In this paper, we try to verify the hypotheses predicted in [7] by axisymmetric simulations in full general relativity. The baseline of the hypotheses predicted in [7] is that the density and angular momentum distribution profiles for the equilibrium stars with $\Gamma \lesssim 4/3$ is significantly different from that for stiff equations of state ($\Gamma \sim 2$), only to which the previous works of the collapse with $q > 1$ have paid attention [9,10,12,13,18–21]. For the soft equations of state, the criterion of black hole formation could be modified. As a first step toward a more realistic simulation, in this paper, we focus on extracting the physical essence for the criterion of black hole formation using simple toy models. We perform simulations for rotating stellar collapse with a *moderately soft* equation of state of $\Gamma = 1.5$ and with a stiff equation of state of $\Gamma = 2$, and compare the results. We illustrate that the global value of q is a good parameter for predicting the direct black hole formation only for the stiff equations of state, not for the soft ones with $\Gamma \lesssim 1.5$. It will be shown that a quasilocal value q_c is a more universal parameter than q for predicting the black hole formation for any equation of state and any rotation law.

The paper is organized as follows. In Sec. II, we briefly describe our formulation, gauge conditions, and boundary conditions. In Sec. III, we describe the initial conditions adopted in this paper and predict the final outcomes of the stellar collapse for our initial models following [7]. Sec. IV presents the numerical results, emphasizing that the predictions made in Sec. III are correct. Sec. V is devoted to a summary. Hereafter, we adopt the geometrical units $G = c = 1$, and Cartesian coordinates $x^k = (x, y, z)$ as the spatial coordinates, with $r = \sqrt{x^2 + y^2 + z^2}$.

II. SUMMARY OF FORMULATION

Fully general relativistic simulations for rotating stellar collapse in axial symmetry are performed using essentially the same formulation as in [24], to which the reader may refer for details and basic equations. The fundamental variables for the hydrodynamics are:

$$\begin{aligned} \rho &: \text{ rest mass density,} \\ \varepsilon &: \text{ specific internal energy,} \\ P &: \text{ pressure,} \\ u^\mu &: \text{ four velocity,} \end{aligned}$$

$$v^i = \frac{dx^i}{dt} = \frac{u^i}{u^t}, \tag{1}$$

where the Latin indices $i, j, k, \cdots$ denote the spatial components of x, y, and z, and the Greek indices $\mu, \nu, \cdots$ the spacetime components. As the variables to be evolved in the numerical simulations, we define a weighted density $\rho_* \equiv \rho \alpha u^t e^{6\phi}$ and a weighted four-velocity $\hat{u}_i \equiv h u_i = (1 + \varepsilon + P/\rho) u_i$ where h denotes the specific enthalpy.

From these variables, the total baryon rest-mass and angular momentum of the system, which are conserved quantities in an axisymmetric spacetime, can be defined as

$$M_* = \int d^3x \rho_*, \tag{2}$$

$$J = \int d^3x \rho_* \hat{u}_\varphi. \tag{3}$$

The general relativistic hydrodynamic equations are solved using a so-called high-resolution shock-capturing scheme [24,25] on the $y = 0$ plane with the cylindrical coordinates (x, z) (in Cartesian coordinates with $y = 0$).

To model initial conditions, we adopt the polytropic equations of state

$$P = K\rho^{1+\frac{1}{n}}, \tag{4}$$

where n is the polytropic index and K polytropic constant. Then physical units enter the problem only through the polytropic constant K, which can be chosen arbitrarily or else completely scaled out of the problem. Thus, in the following we present only the dimensionless quantities which are defined as

$$\begin{aligned} \bar{M}_* = M_* K^{-n/2}, \bar{M} = MK^{-n/2}, \bar{R} = RK^{-n/2}, \\ \bar{J} = JK^{-n}, \bar{\rho} = \rho K^n, \bar{\Omega} = \Omega K^n, \end{aligned} \tag{5}$$

where M, R, and Ω denote the gravitational mass, a radius, and an angular velocity. Hereafter, we adopt the units of $K = 1$ so that we omit the bar.

During the time evolutions, we use the so-called Γ-law equations of state of the form

$$P = (\Gamma - 1)\rho\epsilon, \tag{6}$$

where the adiabatic index Γ is set as $1 + 1/n$. In the absence of shocks, no heat is generated and the collapse proceeds in an adiabatic manner, preserving the polytropic form of the equations of state.

The fundamental variables for the geometry are:

$$\begin{aligned} \alpha &: \text{ lapse function,} \\ \beta^k &: \text{ shift vector,} \\ \gamma_{ij} &: \text{ metric in 3D spatial hypersurface,} \\ \gamma &= e^{12\phi} = \det(\gamma_{ij}), \\ \tilde{\gamma}_{ij} &= e^{-4\phi}\gamma_{ij}, \\ K_{ij} &: \text{ extrinsic curvature.} \end{aligned} \tag{7}$$

As in the series of our papers, we evolve $\tilde{\gamma}_{ij}$, ϕ, $\tilde{A}_{ij} \equiv e^{-4\phi}(K_{ij} - \gamma_{ij}K^k_k)$, and trace of the extrinsic curvature K^k_k together with three auxiliary functions $F_i \equiv \delta^{jk}\partial_j\tilde{\gamma}_{ik}$ with an unconstrained free evolution code as in [12,18,24,26–30].

The Einstein equations are solved in Cartesian coordinates. To impose axisymmetric boundary conditions, the Cartoon method is used [31]: Assuming reflection symmetry with respect to the equatorial plane, simulations are performed using a fixed uniform grid with the grid size $N \times 3 \times N$ in (x, y, z) which covers a computational domain as $0 \le x \le L$, $0 \le z \le L$, and $-\Delta \le y \le \Delta$. Here, N and L are constants and $\Delta = L/N$. The axisymmetric boundary conditions are imposed at $y = \pm\Delta$. Details about the numerical methods as well as the results of longterm and stable test simulations are found in [24] to which the readers may refer.

As the slicing condition we impose an "approximate" maximal slicing condition in which the condition $K^k_k \approx 0$ is imposed [27]. As the spatial gauge, we adopt a dynamical gauge condition proposed in [13,32], with which the shift vector is determined from the equation

$$\partial_t\beta^k = \tilde{\gamma}^{kl}(F_l + \Delta t\partial_t F_l), \tag{8}$$

where Δt denotes the time step in numerical computation. Note that in this gauge condition, β^i obeys a hyperbolic-type equation for a sufficiently small value of Δt because the right-hand side of the evolution equation for F_i contains a vector Laplacian term [26]. The outstanding merit of this gauge condition is that we can save computational time significantly. Furthermore, it has already been illustrated that stable simulations for rotating stellar collapse and merger of binary neutron stars are feasible in this gauge [13,30].

An outgoing wave boundary condition is imposed for $h_{ij}(\equiv \tilde{\gamma}_{ij} - \delta_{ij})$, $\tilde{A}_{ij}$, and F_i at outer boundaries of the computational domain. The condition adopted is the same as that described in [26]. On the other hand, for ϕ and K^k_k, the outer boundary conditions imposed are $r\phi = \text{const}$ and $K^k_k = 0$, respectively.

A black hole may be formed as a result of collapse. We determine the location of it using an apparent horizon finder developed in [33]. As the system approaches a stationary state, the apparent horizon will approach the event horizon. In a dynamical spacetime we compute the apparent horizon mass $M_{\rm AH}$ which is defined as [34]

$$M_{\rm AH} = \sqrt{\frac{A}{16\pi}}, \tag{9}$$

where A denotes area of an apparent horizon.

During the numerical simulations, conservation of the mass and the angular momentum and violation of the Hamiltonian constraint, $H_{\rm error}$, are monitored as code checks. Here, $H_{\rm error}$ is evaluated with a weighted average of the violation by ρ_*

$$H_{\rm error} \equiv \frac{\int \rho_* |V| d^3x}{\int \rho_* d^3x} = \frac{1}{M_*}\int \rho_* |V| d^3x, \tag{10}$$

where V is defined by

$$V \equiv \frac{\tilde{\Delta}\psi - \frac{1}{8}\psi\tilde{R} + 2\pi\psi^5(\rho h w^2 - P) + \frac{\psi^5}{8}\tilde{A}_{ij}\tilde{A}^{ij} - \frac{\psi^5}{12}(K^k_k)^2}{|\tilde{\Delta}\psi| + \frac{1}{8}|\psi\tilde{R}| + 2\pi\psi^5(\rho h w^2 - P) + \frac{\psi^5}{8}\tilde{A}_{ij}\tilde{A}^{ij} + \frac{\psi^5}{12}(K^k_k)^2}. \tag{11}$$

In Eq. (11), $\psi \equiv e^{4\phi}$, $w \equiv \alpha u^t$, and $\tilde{\Delta}$ and $\tilde{R}$ are the Laplacian and the Ricci scalar with respect to the conformal metric $\tilde{\gamma}_{ij}$.

III. INITIAL CONDITIONS AND PREDICTIONS

A. Method of Preparing Initial Conditions

In this paper, we adopt simplified initial conditions following Stark and Piran [10]: We first give a marginally stable spherical polytrope against gravitational collapse, and then, add an angular momentum artificially as well as reduce the pressure to induce the collapse. Selected values for Γ are 1.5, with which an insight into the collapse of stars with moderately soft equations of state will be obtained, and 2, the value that Stark and Piran adopted [10]. Simulations with $\Gamma = 2$ are performed for confirmation of the previous result [10].

In more detail, we generate the initial conditions in the following procedure. First, we give a spherical star which is marginally stable against gravitational collapse, using the polytropic equations of state with $\Gamma = 1.5$ or 2.0. Second, we reduce the pressure to an arbitrarily chosen fraction f_P of its equilibrium pressure. Third, an angular momentum is artificially added according to

$$u_\varphi = e^{4\phi}\varpi^2 u^t \Omega, \quad \text{and} \quad u^t = \sqrt{\frac{-1}{-\alpha^2 + \Omega^2 e^{4\phi}\varpi^2}}, \tag{12}$$

where α and ϕ denote the lapse function and the conformal factor of the spherical polytropes, and Ω is given by

$$\Omega(\varpi) = \Omega_0 \exp\left[-\frac{\varpi^2}{2R_0^2}\right]. \tag{13}$$

Here, $\varpi = \sqrt{x^2 + y^2}$, R_0 is a parameter which controls the degree of differential rotation, and Ω_0 is the angular velocity along the z axis. For $R_0 \to \infty$, the rotation approaches the rigid rotation (we refer to the case with $R_0 \to \infty$ as the rigidly rotating case in the following). Finally, the Hamiltonian and momentum constraints are reimposed by solving the constraint equations, and then the time evolution is set out.

In Tables I and II, we list characteristic quantities for the initial conditions with $\Gamma = 1.5$ and 2.0 used in the present work. $R_S = 6.45$ is a coordinate radius of the marginally stable spherical polytrope with $\Gamma = 1.5$ in the isotropic coordinates. All the quantities are scaled to be nondimensional using the relations (5).

B. Predicting the Final Outcome

Using essentially the same method as described in [7], the final outcome after the collapse for our initial conditions with $q > 1$ is predicted. We pay particular attention to the black hole formation assuming that (i) the collapse proceeds in an axisymmetric manner, (ii) the viscous angular momentum transport during the collapse is negligible, and (iii) the pressure or heating effects never halt the collapse. Because of the assumption that the viscous effect is negligible during the collapse, the specific angular momentum j of each fluid element is conserved in the axisymmetric system. Here, j is defined by

TABLE I. Central density ρ_c, angular velocity of rotational axis Ω_0, differential rotation parameter R_0 (R_S is the coordinate radius of the spherical polytrope in the isotropic coordinates), gravitational mass M, baryon rest-mass M_*, angular momentum J, the nondimensional parameter (spin parameter) $q = J/M^2$, $q_* = J/M_*^2$, and q_c of the initial data for models with $\Gamma = 1.5$ in units of $G = c = K = 1$. f_P denotes a fraction of the initial pressure depletion. "rigid" denotes that rotational velocity field is initially in rigid rotation.

ρ_c	Ω_0	R_0/R_S	M	M_*	J	q	q_*	q_c	f_P
0.005	0.050	∞ (rigid)	0.510	0.530	0.227	0.87	0.81	0.50	0.35
0.005	0.065	∞ (rigid)	0.512	0.535	0.300	1.14	1.05	0.64	0.25
0.005	0.065	1.5	0.501	0.534	0.282	1.08	0.99	0.64	0.25
0.005	0.090	∞ (rigid)	0.529	0.546	0.444	1.59	1.49	0.84	0.1
0.005	0.090	1.0	0.519	0.541	0.377	1.40	1.29	0.86	0.1
0.005	0.090	2/3	0.511	0.537	0.319	1.22	1.11	0.87	0.1
0.005	0.100	∞ (rigid)	0.538	0.552	0.512	1.77	1.68	0.91	0.01
0.005	0.100	1.0	0.524	0.545	0.427	1.55	1.44	0.94	0.01
0.005	0.100	2/3	0.514	0.540	0.358	1.36	1.23	0.96	0.01
0.005	0.115	∞ (rigid)	0.562	0.563	0.640	2.03	2.02	1.01	0.01
0.005	0.115	1.0	0.540	0.553	0.515	1.77	1.68	1.05	0.01
0.005	0.115	2/3	0.526	0.546	0.319	1.54	1.42	1.08	0.01

TABLE II. The same as Table I but for models with $\Gamma = 2.0$.

ρ_c	Ω_0	R_0	M	M_*	J	q	q_*	q_c	f_P
0.318	0.65	∞ (rigid)	0.179	0.197	0.0364	1.13	0.93	0.90	0.01
0.318	0.67	∞ (rigid)	0.182	0.199	0.0383	1.16	0.97	0.91	0.01
0.318	0.68	∞ (rigid)	0.183	0.199	0.0393	1.17	0.99	0.92	0.01

$$j \equiv h u_\varphi. \tag{14}$$

Then, we define a rest-mass distribution $m_*(j)$ as a function of j, which is the integrated baryon rest-mass of fluid elements with the specific angular momentum less than j:

$$m_*(j) \equiv 2\pi \int_{j'<j} \rho_* r^2 dr d(\cos\theta). \tag{15}$$

Similarly, a specific angular momentum distribution is defined according to

$$J(j) \equiv 2\pi \int_{j'<j} \rho_* j' r^2 dr d(\cos\theta). \tag{16}$$

Gauge independency and conservation of these distribution functions come from the axial symmetry (the existence of the rotational Killing vector field) and can be proven by the hydrodynamical equations

$$\frac{\partial \rho_*}{\partial t} + \frac{\partial(\rho_* v^I)}{\partial x^I} = 0, \tag{17}$$

$$\frac{\partial(\rho_* j)}{\partial t} + \frac{\partial(\rho_* j v^I)}{\partial x^I} = 0, \tag{18}$$

where the index I denotes the component of ϖ and z.

For the following analysis, it is better to define a quasilocal gravitational mass since in contrast with the case of the soft equations of state ($\Gamma \lesssim 4/3$) studied in [7], stars are compact with $R/M \lesssim 15$, and hence, difference between the rest-mass and the gravitational mass is not negligible (see Table I). However, the gravitational mass cannot be locally defined in general relativity. Thus, here, assuming that the ratio of the "quasilocal gravitational mass" to the rest-mass is uniform inside a star, we define a "gravitational mass distribution" as

$$m(j) \equiv \frac{M}{M_*} m_*(j). \tag{19}$$

Note that $m(j)$ is equal to M for a maximum value of j (hereafter $j_{\max}$) and that for $\Gamma \approx 4/3$, $m(j)$ is approximately identical with $m_*(j)$.

From these distribution functions, we define spin parameter distributions as

$$q_*(j) \equiv \frac{J(j)}{m_*(j)^2} \quad \text{and} \quad q(j) \equiv \frac{J(j)}{m(j)^2}. \tag{20}$$

These may be approximately regarded as the spin parameters of an inner region composed of fluid elements with the specific angular momentum less than j. Although it is not clear which of the two spin parameters is better for the analysis, we adopt $q(j)$ because of the following reasons: (i) since $q(j)$ is equal to the global quantity q for $j = j_{\max}$, $q(j)$ would be the better quantity for a large value of j; (ii) M_* is always larger than M for all the models. (This is likely to be the case for all the stable stars.) This implies that $q(j) > q_*(j)$. As a result, for $q(j) < 1$, $q_*(j)$ is also smaller than unity.

In Figs. 1(a), 2(a), 3(a), and 4, $q(j)$ as a function of $m_*(j)/M_*$ are displayed for the models with $\Gamma = 1.5$ listed in Table I. Figure 5 also shows the same relation for models with $\Gamma = 2.0$ listed in Table II. These figures indicate that the values of $q(j)$ and $q_*(j)$ at the center of stars (hereafter denoted as q_c and $q_{*,c}$) can be much smaller than unity even if the global values of q (or $q_*(j_{\max})$ which is hereafter denoted by q_*) are larger than unity. An outstanding difference between the results

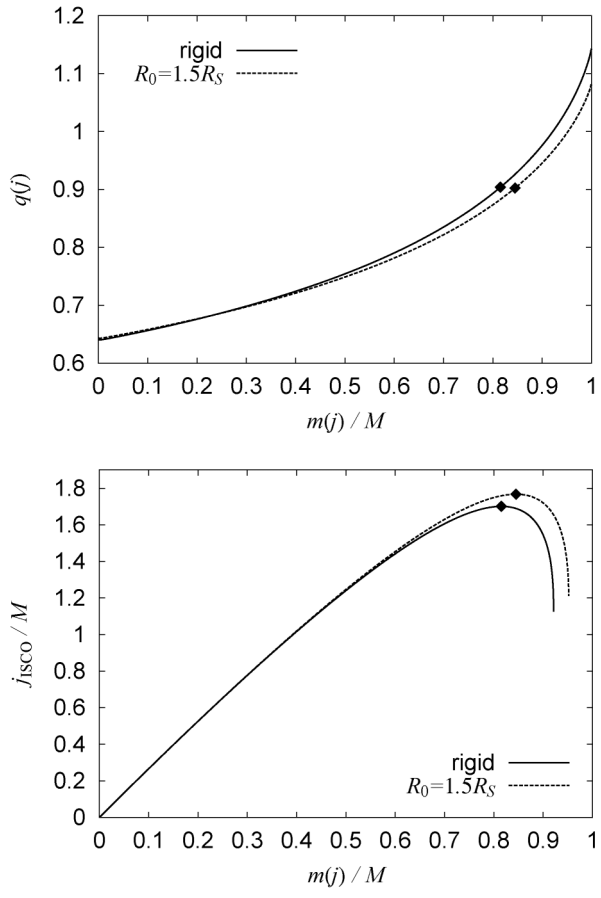

FIG. 1. (a) The distribution of $q(j)$ and (b) $j_{\rm ISCO}$ as a function of $m(j)/M[= m_*(j)/M_*]$ for models with $\Omega_0 = 0.065$ and for $\Gamma = 1.5$. The solid and dashed curves denote the results for rigid rotation and differential rotation with $R_0 = 1.5R_S$, respectively. The filled diamonds indicate values of $m(j)/M[= m_*(j)/M_*]$ and $q(j)$ at the maximum value of $j_{\rm ISCO}$.

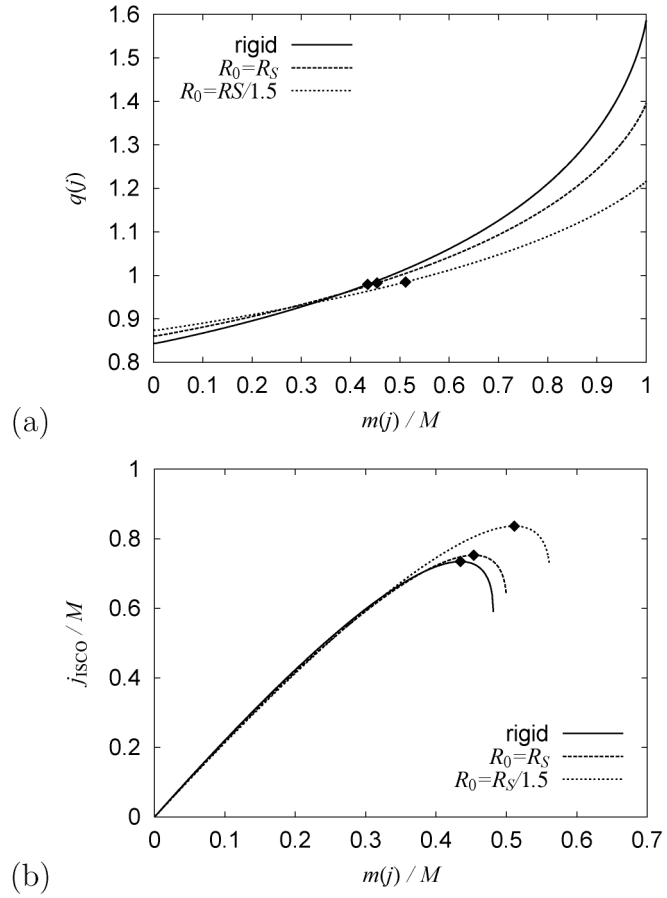

FIG. 2. The same as Fig. 1 but for $\Omega_0 = 0.090$. The solid, dashed, and dotted curves denote the results for rigid rotation, differential rotation with $R_0 = R_S$, and with $R_0 = R_S/1.5$, respectively.

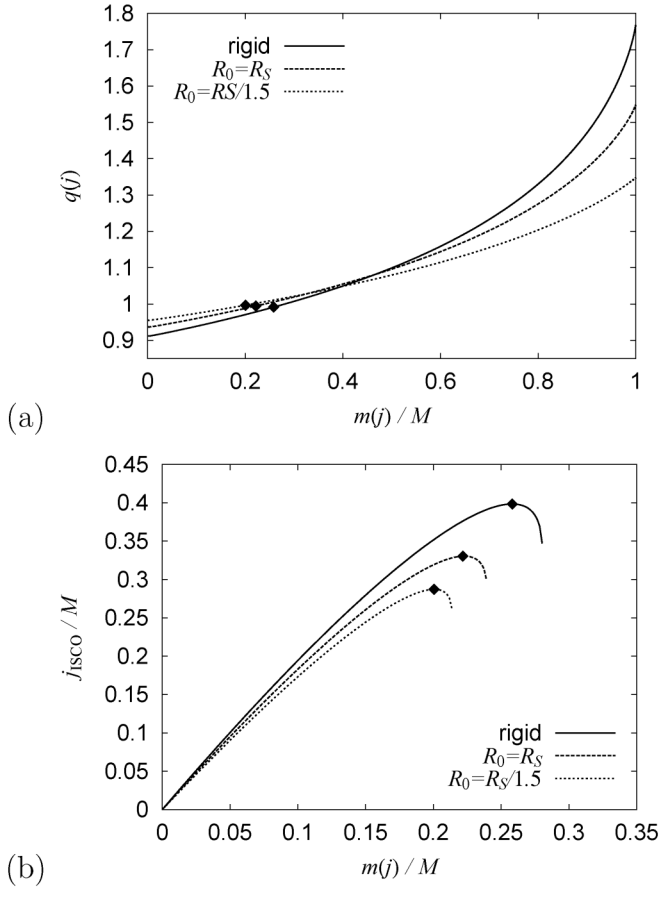

FIG. 3. The same as Fig. 2 but for model of $\Omega_0 = 0.100$.

for two values of Γ is found in the ratio of q/q_c for the rigidly rotating case; $q/q_c \approx 2$ for $\Gamma = 1.5$, while ≈ 1.25 for $\Gamma = 2$. (Note that for $\Gamma \approx 4/3$, $q/q_c \approx 2.5$.) This difference results from the fact that for softer equations of state, the star has a more centrally-condensed structure.

As the collapse proceeds, an inner region of the star will collapse faster. This property will be more outstanding for the softer equations of state since the stars have more centrally-condensed structures. Taking these predictions and the profile of $q(j)$ into account, we assume that the inner region in which $q(j) < 1$ may collapse first to form a "seed" black hole. Assuming that a seed black hole is formed during the collapse, we predict the subsequent evolution in the following manner. Here, we focus only on the rapidly rotating case with a large value of $q > 1$ but with $q_c < 1$. Since the centrifugal force of the rapidly rotating progenitors is large enough, the collapse in an early stage will dominantly proceed in the z direction to be a disklike structure. The formed disk will subsequently collapse to form a black hole. In a formed disk, fluid elements at the same cylindrical radius are likely to have an approximately identical value of the specific angular momentum j. Therefore, the fluid elements of the same value of j will simultaneously collapse or fall into the black hole even if they are initially at different locations.

Now, let us consider innermost stable circular orbit (ISCO) around the growing seed black hole located at

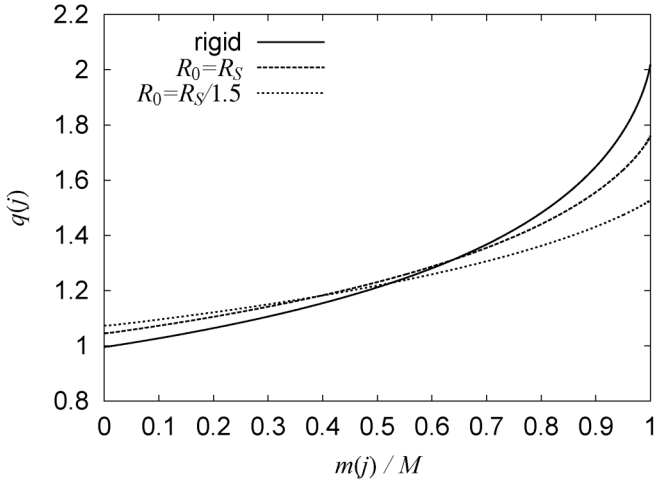

FIG. 4. The same as Fig. 2(a) but for model of $\Omega_0 = 0.115$.

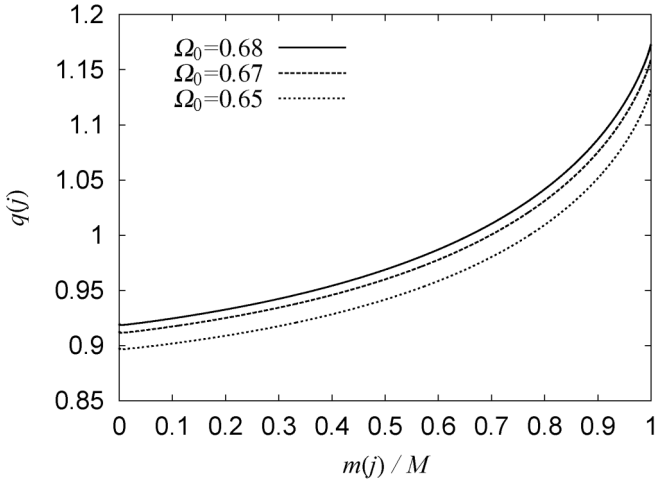

FIG. 5. The same as Fig. 4 but for rigidly rotating models with $\Gamma = 2.0$. The solid, dashed, and dotted curves denote the results for $\Omega_0 = 0.68$, 0.67, and 0.65, respectively.

the center. If the value of j of a fluid element is smaller than that at the ISCO, $j_{\rm ISCO}$, the element will fall into the seed black hole eventually. In fact, there is a possibility that some fluid elements can be captured even for $j > j_{\rm ISCO}$ if it is on a noncircular orbit. Ignoring such trajectories yields the minimum amount of fluid elements that will fall into the black hole. The value of $j_{\rm ISCO}$ will change as the ambient fluid elements accrete onto the seed black hole. If $j_{\rm ISCO}$ increases as a result of the accretion, the more ambient fluid elements will fall into the black hole. On the other hand, if $j_{\rm ISCO}$ decreases during the accretion, no more fluid element will fall into the black hole, and as a result, the dynamical growth of the black hole will terminate. The above speculation suggests that the evolution of the baryon mass $m_*(j)$ and the angular momentum $J(j)$ enclosed inside the seed black hole will be approximately determined by the initial distribution of $m_*(j)$ and $J(j)$ if all viscous effects such as angular momentum transfer are negligible.

To estimate the value of $j_{\rm ISCO}$ and to predict the growth path of the seed black hole, we assume that the spacetime metric can be instantaneously approximated by that of a Kerr spacetime of the mass $m(j)$ and the spin $q(j)$. On these approximations, we can compute $j_{\rm ISCO}$ of a seed black hole as [35–37],

$$j_{\rm ISCO} = \frac{\sqrt{m(j) r_{\rm ISCO}}[{r_{\rm ISCO}}^2 - 2q(j)m(j)\sqrt{m(j) r_{\rm ISCO}} + [q(j)m(j)]^2]}{r_{\rm ISCO}[{r_{\rm ISCO}}^2 - 3m(j) r_{\rm ISCO} + 2q(j)m(j)\sqrt{m(j) r_{\rm ISCO}}]^{1/2}}, \tag{21}$$

where

$$r_{\rm ISCO} = m(j)[3 + Z_2 - \{(3 - Z_1)(3 + Z_1 + 2Z_2)\}^{1/2}],$$
$$Z_1 = 1 + [1 - q(j)^2]^{1/3}[\{1 + q(j)\}^{1/3} + \{1 - q(j)\}^{1/3}],$$
$$Z_2 = [3q(j)^2 + Z_1^2]^{1/2}.$$

Here, $m(j)$ and $q(j)$ are not strictly the gravitational mass and the spin parameter. We guess that they may have a systematic error of magnitude $|\Delta m|/m = |1 - (m_*/m) \times (M/M_*)| \lesssim |1 - M/M_*|$ for the mass and $|\Delta q|/q \lesssim 2|1 - M/M_*|$ for the spin parameter. This implies that the value of $j_{\rm ISCO}$ determined by Eq. (21) will also include a systematic error. The magnitude of the error for $j_{\rm ISCO}$ may be $\lesssim 10\%$ (see Table I).

In Figs. 1(b), 2(b), and 3(b), we show $j_{\rm ISCO}[m(j), q(j)]$ as a function of $m(j)/M$ for the models with $\Gamma = 1.5$. These figures show that for the models in which the degree of differential rotation is not too high, $j_{\rm ISCO}$ has a maximum (hereafter denoted as $j_{\rm ISCO:max}$). Thus, we predict that the seed black hole will grow until j reaches $j_{\rm ISCO:max}$. In Table III, we show $j_{\rm ISCO:max}/M$, $m(j_{\rm ISCO:max})/M$, and $q(j_{\rm ISCO:max})$ for $\Gamma = 1.5$. Note that for models of $\Omega_0 = 0.115$ in which $q_c > 1$, we predict that no seed black hole is formed.

Here, $m(j_{\rm ISCO:max})/M$ and $q(j_{\rm ISCO:max})$ may be approximately regarded as the mass fraction $M_{\rm BH}/M$ and the spin parameter $q_{\rm BH}$ of the final black hole (which is in a quasistationary state), namely,

$$M_{\rm BH} \approx m(j_{\rm ISCO:max}), \tag{22}$$

$$q_{\rm BH} \approx q(j_{\rm ISCO:max}). \tag{23}$$

This approximate estimate suggests that an appreciably massive disk ($M_{\rm disk}/M = 0.1 \sim 0.8$) will be formed eventually. Note that $M_{\rm BH}$ and $q_{\rm BH}$ computed above might include a systematic error because of the reason that we approximate a spacetime composed of a black hole and a massive disk simply as a Kerr spacetime. However, $j_{\rm ISCO}$ is likely to be determined from the local quantities near

TABLE III. The maximum values of $j_{\rm ISCO}$, and corresponding values of $m_*(j_{\rm ISCO})/M_*$ and $q(j_{\rm ISCO})$ for $\Gamma = 1.5$ initial models of $\Omega_0 = 0.050$, 0.065, 0.090, and 0.100.

Ω_0	R_0	$j_{\rm ISCO:max}/M$	$m_*(j_{\rm ISCO:max})/M_*$	$q(j_{\rm ISCO:max})$
0.050	∞ (rigid)	2.29	0.953	0.792
0.065	∞ (rigid)	1.70	0.815	0.904
0.065	$R_S/1.5$	1.77	0.845	0.902
0.090	∞ (rigid)	0.734	0.435	0.979
0.090	R_S	0.753	0.454	0.982
0.090	$1.5R_S$	0.836	0.511	0.984
0.100	∞ (rigid)	0.399	0.256	0.992
0.100	R_S	0.330	0.222	0.995
0.100	$1.5R_S$	0.287	0.201	0.997

the black hole and, hence, we consider that our treatment may be approximately correct.

It is found that for a fixed value of q_c, the corresponding value of $q(j_{\rm ISCO:max})$ is almost independent of the differential rotation parameter R_0, i.e., the value of q. This suggests that the spin parameter of the final state of the black hole may be determined by the value of q_c and independent of q as far as $q(j)$ is an increasing function of j.

In summary, we have predicted the following facts in this section: (I) even if the global spin parameter q significantly exceeds unity, an inner region of a star with $q_c < 1$ will collapse first to form a seed black hole;, i.e., the black hole formation will be determined by the local value q_c independent of the global value of q. On the other hand, for $q_c > 1$, no black hole will be formed; (II) the formed seed black hole will grow as the ambient fluid subsequently accretes onto it; (III) the evolution of the relation between the rest-mass m_* and angular momentum J enclosed inside the growing seed black hole will agree approximately with the initial relation between $m_*(j)$ and $J(j)$; (IV) the final outcome of the dynamical collapse of a star with $q_c < 1$ is a black hole surrounded by a disk.

These predictions made from the analysis of the initial conditions are quite reasonable, but they are nothing but predictions. Thus, to confirm them, it is obviously necessary to perform fully general relativistic simulations. In the next section, we present the results of numerical simulations and verify the predicted facts.

IV. RESULTS OF NUMERICAL SIMULATION

A. Results for $\Gamma = 1.5$

We performed simulations for the various initial models listed in Table I, varying grid spacing as $\Delta x = 0.018$, 0.015, 0.01125, 0.009, and 0.006 (in units of $G = c = K = 1$). In the simulations, the uniform grid is adopted and the outer boundaries along the x and z axes are located at $L \gtrsim 10 \gtrsim 20M$. Simulations were performed changing the location of the outer boundaries, but we found that the numerical results depend very weakly on the location. Numerical results could be affected by the location of the outer boundaries in a very longterm simulation [38]. However, in the present paper, the timescale of black hole formation is much shorter than the timescale in which effects from the outer boundaries located at a finite radius are amplified. Numerical simulations were performed on FACOM VPP5000 in the data processing center of the National Astronomical Observatory of Japan, and personal computers with Pentium-4 processors, each of which has 2 Gbytes memory and a 3.0 GHz clock.

In Figures 6(a) and 6(b) we display the evolution of the central value of ρ_* (denoted as $\rho_{*,c}$) and the central value of the lapse function α_c for the differentially rotating

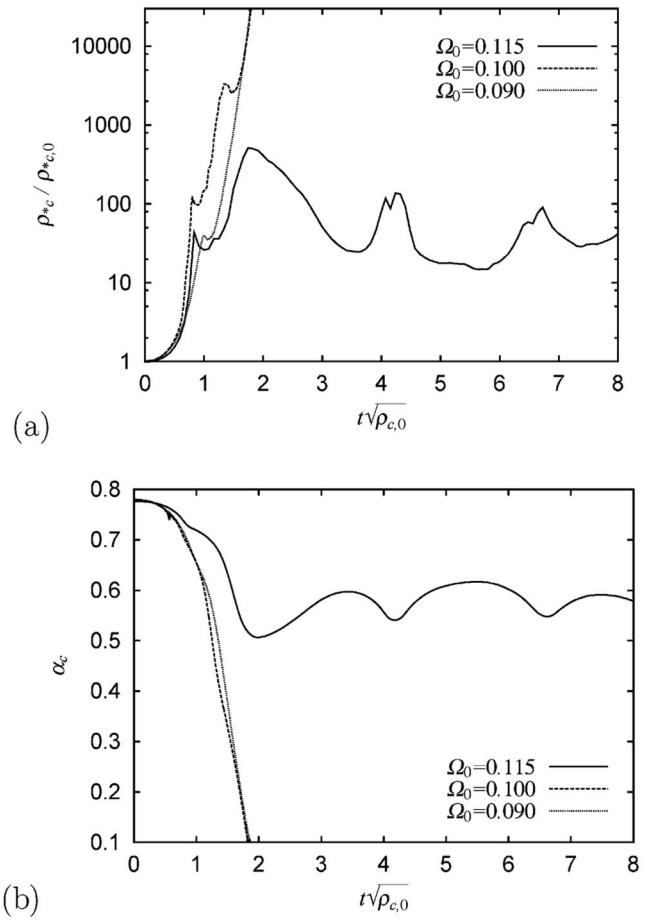

FIG. 6. Evolution of (a) the central density $\rho_{*,c}$ and (b) the central value of the lapse function α_c for $\Gamma = 1.5$. In both figures, the solid, dashed, and dotted curves denote the differentially rotating models of $R_S = R_0/1.5$ with $\Omega_0 = 0.090$, 0.100, and 0.115 ($q_c = 0.87$, 0.96, and 1.08), respectively. All the results are obtained with $\Delta x = 0.006$. Here, $\rho_{c,0}^{-1/2} \sim 25M$.

models with $\Gamma = 1.5$, $R_S = R_0/1.5$, and $\Omega_0 = 0.090$, 0.100, and 0.115. The grid resolution adopted for all these simulations is $\Delta x = 0.006$. A convergent result is obtained for the models of $\Omega_0 = 0.090$ and 0.115 even for $\Delta x = 0.009$. For the model of $\Omega_0 = 0.100$, we should be careful since the formed black hole is very small and thus a highly accurate grid resolution is required to follow the black hole formation. In this case, in simulations with coarse grid resolutions, we may conclude that a black hole is not formed. However, for $\Delta x \lesssim 0.009$, we have found that a black hole is formed. Thus, for all the models with $q_c < 1$ ($\Omega_0 \leq 0.100$), the collapse proceeds to form an apparent horizon irrespective of the values of q. It is clearly illustrated that even if the value of q is much larger than unity, a black hole may be formed for $q_c < 1$. These results are obviously counterexamples of the previous criterion, $q > 1$, for no black hole formation.

For all the models with $\Omega_0 = 0.115$ for which $q_c > 1$, on the other hand, we find that black hole is not formed

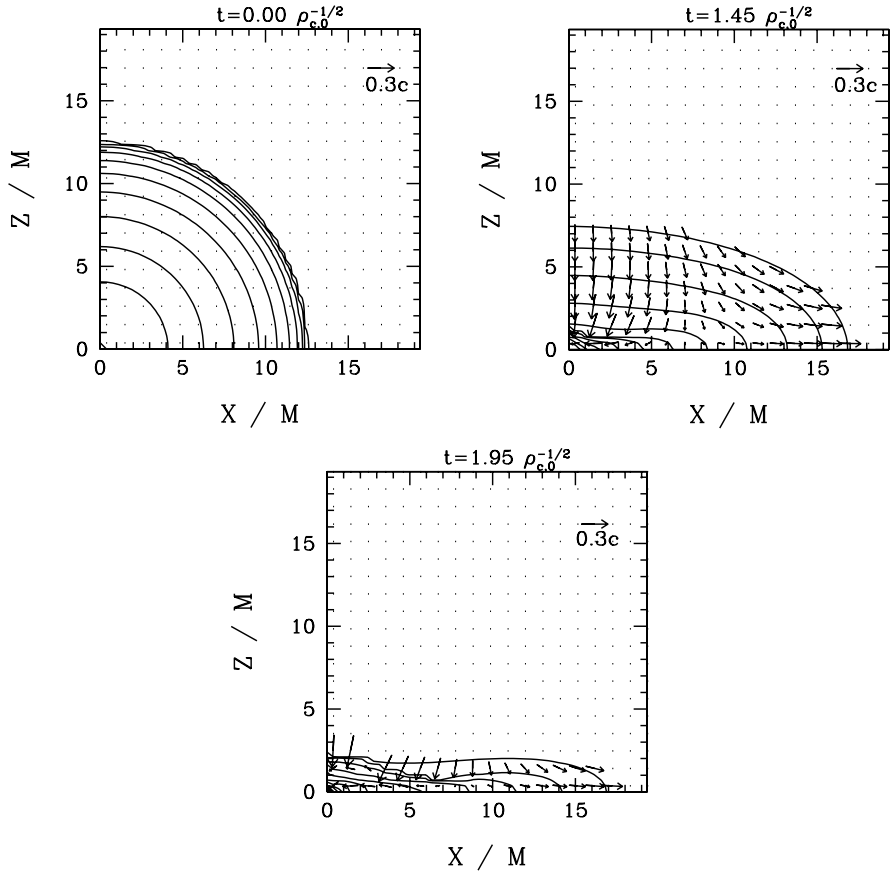

FIG. 7. Snapshots of the density contour curves of ρ_* and of the velocity field of (v^x, v^z) at selected time slices for the rigidly rotating model with $\Omega_0 = 0.065$. The contour curves are drawn for $\rho_* = \rho_a \times 10^{-0.5j}$, with $j = 0, 1, 2, \cdots, 10$, where $\rho_a = 0.011$, 1, and ten at $t\rho_{c,0}^{1/2} = 0$, 1.45, and 1.95. The small thick solid circle with the radius $\sim 0.2M$ of the last panel denotes the apparent horizon.

and that the stars experience bounces and oscillation. This results from the fact that the centrifugal force near the rotational axis is too strong to form a seed black hole.

In Figs. 7 and 8, we plot snapshots of the contour curves of ρ_* and of the velocity field of (v^x, v^z) at selected time slices for the rigidly rotating model with $\Omega_0 = 0.065$ and for the differentially rotating model with $\Omega = 0.115$ and $R_0 = R_S/1.5$. As we predicted in Sec. III, the collapse first proceeds in the direction of the rotational axis (z axis) to be a disklike structure. Then, the formed disk collapses to the center to form a black hole for $q_c < 1$. Irrespective of the degree of differential rotation, the collapse proceeds in essentially the same manner and a seed black hole is formed. For $q_c > 1$, the centrifugal force is strong enough to prevent black hole formation. In this case, an oscillating disk is the outcome after the collapse (see Fig. 8). Such a disk may be unstable against a nonaxisymmetric instability (e.g., [19,28]).

Even if the value of q is much larger than unity, a black hole is formed for models with $q_c < 1$, as predicted in Sec. III. To confirm this conclusion strictly, we performed convergence tests varying the grid resolution for a wide range. In Figs. 9(a)–9(c) we show $H_{\rm error}$ and the central density $\rho_{*,c}$ with different grid spacing ($\Delta x = 0.009$, 0.015, and 0.018) for $\Omega_0 = 0.065$ and $R_0 = 1.5R_S$. Figure 9(a) shows that the accuracy is improved with decrease of the grid spacing. To clarify at what order the convergence is achieved, in Fig. 9(b), we plot the ratio of $H_{\rm error}$ of $\Delta x = 0.015$ and 0.018 to that of 0.009. It is found that the magnitude of the error for $\Delta x = 0.015$ and 0.018 is about 4–5 and 7–9 times as larger as that for $\Delta x = 0.009$ for $t \lesssim \rho_{c,0}^{-1/2}$. This implies that the third-order convergence is approximately achieved. This seems to be because our hydrodynamical scheme is of the third-order accuracy in space in the absence of shocks [24] and because $H_{\rm error}$ is defined with a weight factor ρ_* (cf., Eq. (10)). For $t \gtrsim 1.2\rho_{c,0}^{-1/2}$, the convergence changes from the third to the *first* order fairly rapidly. This is because for such late time, shocks are formed, and around shocks, transport terms in the hydrodynamic equations are computed using a first-order scheme. After the shock

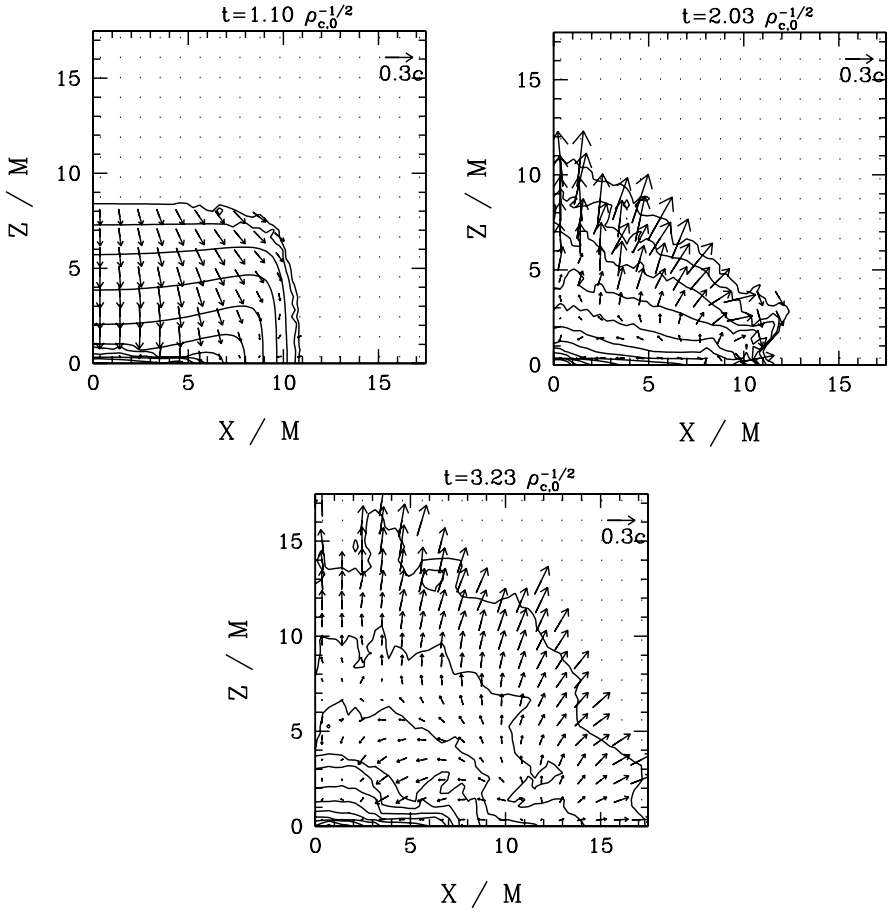

FIG. 8. The same as Figs. 7 but for the differentially rotating model with $\Omega_0 = 0.115$ and $R_0 = R_S/1.5$. The contour curves are drawn for $\rho_* = \rho_a \times 10^{-0.5j}$, with $j = 0, 1, 2, \cdots, 10$ where $\rho_a = 1$ for all the time steps.

formation, shock waves propagate in a wide region of a collapsed star, and as a result, the order of the convergence factor eventually relaxes to the first order.

To accurately determine the threshold values of q_c or q, it is also crucial that the rest-mass distribution $m_*(j)$ as a function of the specific angular momentum is conserved [39] accurately at least until the first formation of an apparent horizon. In Figs. 10(a) and 10(b) we compare the rest-mass distribution at $t = 0$ and at the first formation of apparent horizon for the rigidly rotating case with $\Omega_0 = 0.065$ and 0.090. These figures demonstrate that the rest-mass distribution $m_*(j)$ is conserved well, implying that a spurious numerical transfer of the angular momentum is small.

For all the models with $\Omega_0 = 0.100$ in which $q_c \approx 0.91$–0.96, we find that a seed black hole is formed. However, in this case, it is not easy to obtain the convergent result for $M_{\rm AH}$, say within 10% error, in the present computational setting because of the restriction of the grid resolution. Numerical experiments have told us that the grid spacing to follow the black hole formation should be smaller than $\sim 0.1 M_{\rm seed,AH}$ (not $\Delta x \lesssim 0.1M$), with which the black hole horizon is covered by ~ 10 grid points. For the model with $\Omega_0 = 0.100$, we found that mass of the seed black hole is $M_{\rm seed,AH} \lesssim 0.1M$. This implies that for this model, the required grid spacing is $\Delta x \lesssim 0.1 M_{\rm seed,AH} \lesssim 0.01M \approx 0.005$. This value is nearly equal to the finest grid spacing that we adopted in this work.

In Figs. 11(a) and 11(b) we show the time evolution of the apparent horizon mass for the rigidly rotating models with $\Omega_0 = 0.065$ and 0.090. These figures indicate that the black hole evolution can be divided into two phases. One is a phase in which a seed black hole is formed at the central region. The other is a phase in which the seed black hole grows as the ambient fluid falls into it. We define the mass of the seed apparent horizon $M_{\rm AH,seed}$ from the location of the break of the curves for $M_{\rm AH}(t)$. Then, it is found that $M_{\rm AH,seed}$ is much smaller than the total mass of the system M and $M_{\rm BH}$ defined in Eq. (22). As a reasonable result, it is also found that $M_{\rm AH,seed}$ is smaller for the larger value of Ω_0 and R_0 (i.e., for the more rapidly and more rigidly rotating cases). Note that at the accretion phase, the system is composed of a black hole and a surrounding massive disk accreting onto the central black hole (see Fig. 7).

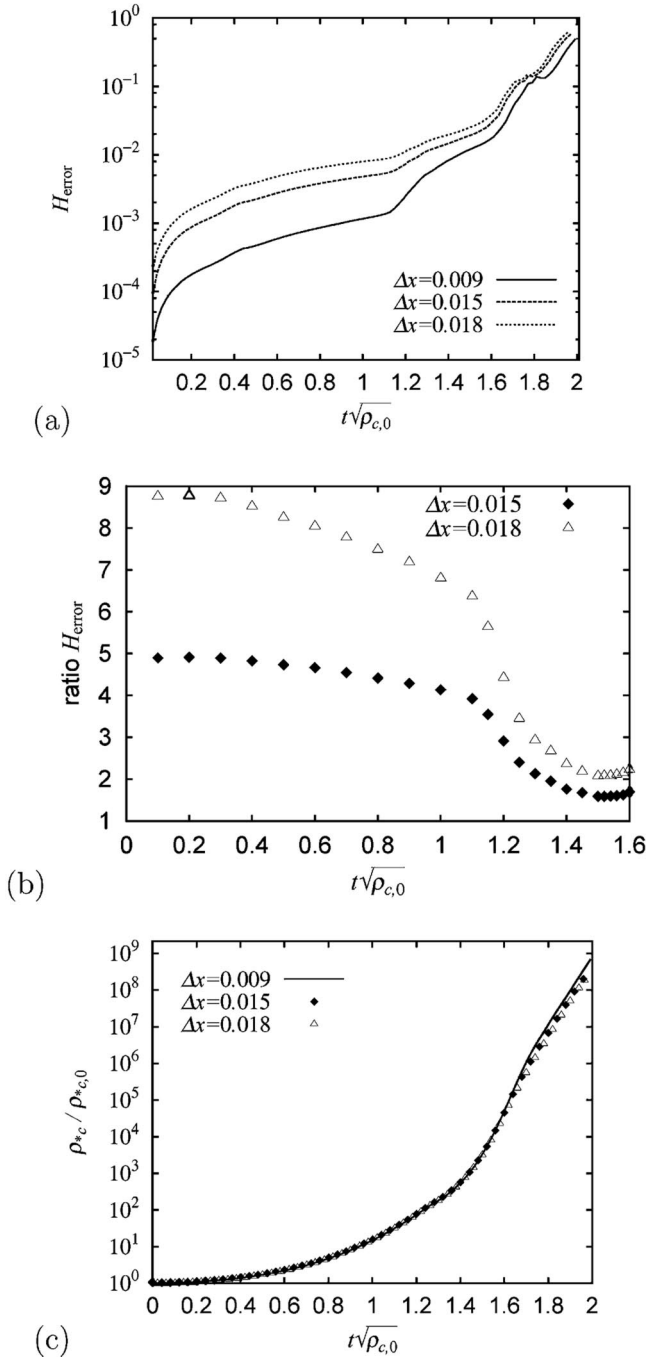

FIG. 9. (a) Violation of the Hamiltonian constraint $H_{\rm error}$, (b) ratio of the violation $H_{\rm error}(\Delta x = 0.015)/H_{\rm error}(\Delta x = 0.009)$ and $H_{\rm error}(\Delta x = 0.018)/H_{\rm error}(\Delta x = 0.009)$, and (c) the central value of ρ_* ($\rho_{*,c}$) as a function of time for $\Omega_0 = 0.065$ and $R_0 = 1.5R_S$. In panel (a), the solid, dashed, and dotted curves denote the results of $\Delta x = 0.009$, 0.015, and 0.018. In panel (b) and (c), the filled diamonds and the open triangles denote the results of $\Delta x = 0.015$ and 0.018.

For a Kerr black hole of the mass $M_{\rm BH}$ and the spin parameter $q_{\rm BH}$, the irreducible mass of the event horizon $M_{\rm irr}$ is defined as [6]

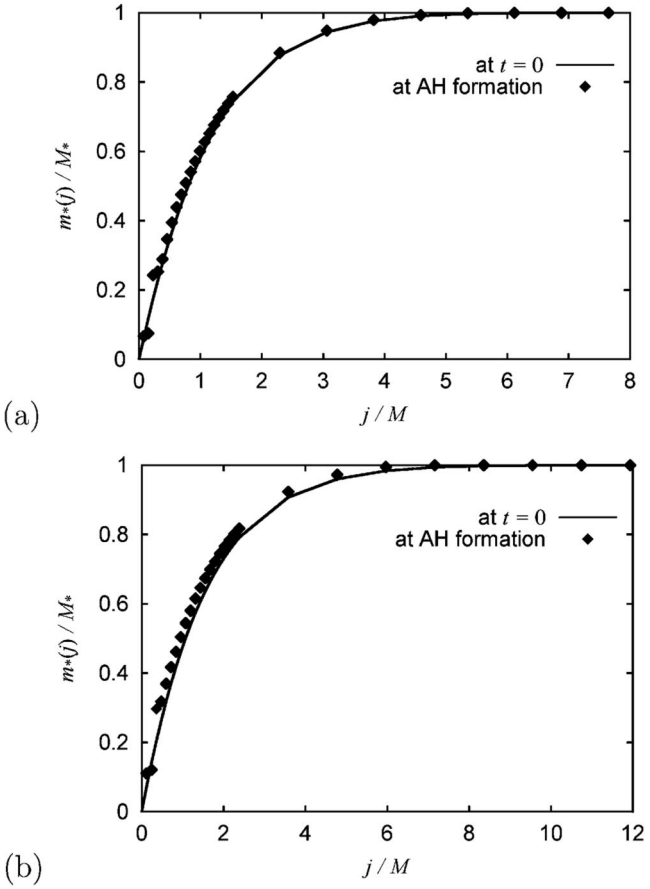

FIG. 10. Rest-mass distribution as a function of specific angular momentum j (a) for the rigidly rotating models with $\Omega_0 = 0.065$ and (b) for $\Omega_0 = 0.090$. In both panels, the solid curves denote the initial rest-mass distributions and the filled diamonds the rest-mass distributions when an apparent horizon is first formed. The grid resolution is $\Delta x = 0.01125$ for (a) and $\Delta x = 0.006$ for (b).

$$(M_{\rm irr}[M_{\rm BH}, q_{\rm BH}])^2 \equiv \frac{1}{2}M_{\rm BH}^2[1 + \sqrt{1 - q_{\rm BH}^2}]. \qquad (24)$$

Provided that the final state of the black hole may be approximated as a Kerr black hole (even though it is surrounded by an appreciable disk), $M_{\rm AH}$ should asymptotically approach $M_{\rm irr}[M_{\rm BH}, q_{\rm BH}]$. Assuming that $M_{\rm BH}$ and $q_{\rm BH}$ may be evaluated from the approximate relations (22) and (23), $M_{\rm irr}/M$ is ≈ 0.69, 0.72, 0.34, and 0.39 for $(\Omega_0, R_0) = (0.065, \infty)$, $(0.065, 1.5R_S)$, $(0.090, \infty)$, and $(0.090, 2R_S/3)$, respectively, (see the horizontal lines in Fig. 11).

For $\Omega_0 = 0.065$ (the solid curves in Fig. 11(a)), $M_{\rm AH}$ appears to approach the irreducible mass. For $\Omega_0 = 0.090$, on the other hand, the computation crashes in the middle of the black hole evolution. To carry out a simulation beyond this time, the so-called black hole excision techniques [22] are necessary. As far as we know, however, all groups [19,20] which performed simulations of rotating stellar collapse have adopted the so-called simple

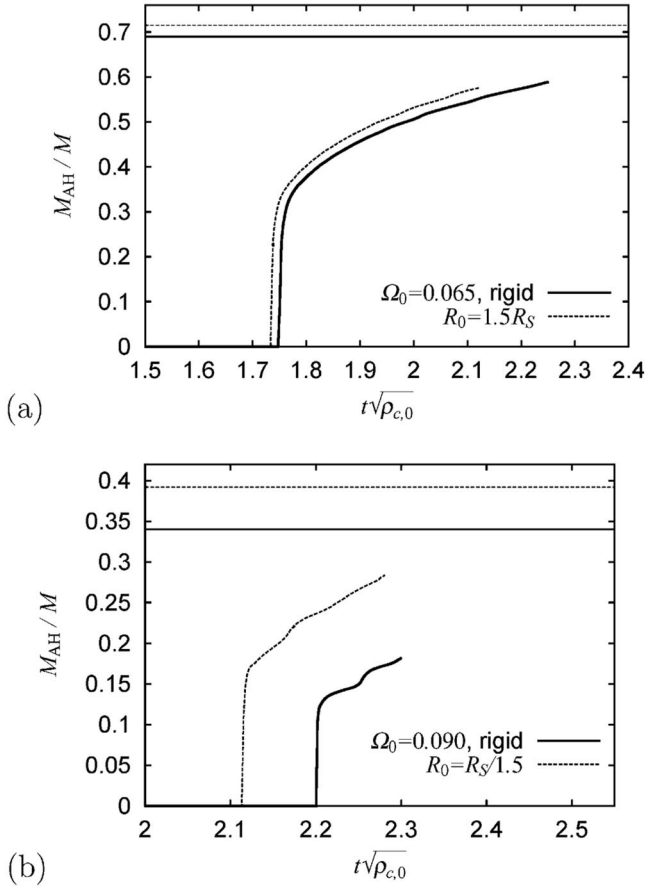

FIG. 11. Evolution of the apparent horizon mass $M_{\rm AH}$ for the rigidly rotating models with (a) $\Omega_0 = 0.065$ and (b) $\Omega_0 = 0.090$. In both panels, the horizontal lines denote the irreducible mass $M_{\rm irr}$ which is $\approx 0.69M$ and $0.72M$ for $(\Omega_0, R_0) = (0.065, \infty)$ and $(0.065, 1.5R_S)$, and $\approx 0.34M$ and $0.39M$ for $(\Omega_0, R_0) = (0.090, \infty)$ and $(0.090, 2R_S/3)$.

excision technique developed by Alcubierre and Brügmann [23]. This method will be robust for nearly stationary systems because the boundary conditions near the black hole horizon are imposed in terms of the time derivatives for the geometric variables. For the collapse of a marginally stable polytrope with a stiff equation of state (with $\Gamma \gtrsim 5/3$), all the matter collapse to a black hole rather simultaneously. In such cases, the system settles down to a stationary black hole fairly quickly after the first formation of the apparent horizon [13]. Thus, the simple excision technique is likely to work. However, in other cases such as the collapse of a marginally stable star with soft equations of state, the collapse does not proceed simultaneously, and hence, the system does not settle down to a stationary state soon after the first formation of a black hole. As illustrated in this paper, in such collapse, a seed black hole of small mass is first formed, and then, it grows gradually as a result of accretion of the surrounding matter. During the growth of the black hole, the system is dynamical, and hence, there is no reason that the simple excision technique works well. Actually, our recent numerical experiments have indicated that it is difficult to perform accurate simulations for the collapse with soft equations of state using the simple excision technique [40]. Thus, we suspect that there may be no fully general relativistic implementation with the black hole excision techniques which is applicable for problems with *soft equations of state* (with $\Gamma \lesssim 1.5$). Developing such an implementation is an issue for the future. We note that numerical instabilities that may be associated with the simple excision are also reported in simulations of dynamical black hole spacetimes (e.g., [41–43]).

To confirm prediction (IV), it will be necessary to continue simulations for a long time $>100M$ after the formation of apparent horizons. Unfortunately, the computations crash in $\sim 20M$ after the first formation of apparent horizons, due to the grid stretching around the black hole horizons, and thus, we cannot confirm this prediction strictly. Although some implementations with a black hole excision code are in operation, they are applicable only for stiff equations of state and for the duration of $<100M$ [19,20]. Again, it is necessary to develop a robust excision technique to confirm the prediction (IV).

Although simulations do not clarify the final state of the collapse, the above results strongly suggest that the final outcome of the dynamical collapse of a rotating star with $q > 1$ and $q_c < 1$ is a black hole surrounded by a massive disk of mass of order $0.1M$. We also note that $M_{\rm AH,seed}$ is always smaller than $M_{\rm irr}$ by a factor of ~ 2. This implies that the black hole significantly grows during the accretion phase.

From the above results, we have confirmed the predictions (I) and (II) suggested in Sec. III B: We have found that $q_c \approx 1$ is an approximate threshold for the black hole formation and that after its formation, the seed black hole significantly grows due to accretion.

To confirm the prediction (III), we compute the evolution of the total baryon rest-mass and the total angular momentum enclosed inside an apparent horizon (denoted as $m_{*,\rm AH}(j)$ and $J_{\rm AH}(j)$, respectively) and compare the relation between them with the initial one between $m_*(j)$ and $J(j)$. In Fig. 12(a), we display evolution of $m_{*,\rm AH}(j)$ and $J_{\rm AH}(j)$ (the diamonds) together with the initial relation (the solid curve) for the rigidly rotating model with $\Omega_0 = 0.065$. It is found that the evolutionary track of the black hole is approximately determined by the initial distribution of the mass and the angular momentum, until a numerical error is accumulated significantly. To confirm this result more firmly, we also performed a simulation for a moderately rapidly rotating star (rigid rotation with $\Omega_0 = 0.050$). In Fig. 12(b), we show the evolution track of $m_{*,\rm AH}(j)$ and $J_{\rm AH}(j)$ together with the initial distribution for this case. It is found that the initial distribution approximately determines an evo-

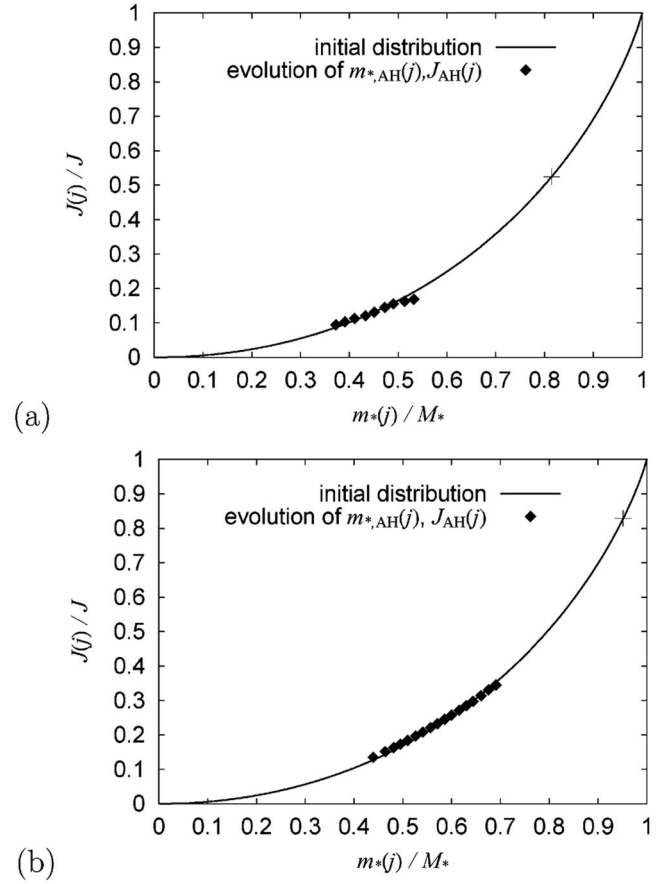

FIG. 12. Evolution of the baryon rest-mass $m_{*,\mathrm{AH}}$ and the angular momentum J_{AH} enclosed inside apparent horizons (filled diamonds) for the rigidly rotating models with (a) $\Omega_0 = 0.065$ and (b) $\Omega_0 = 0.050$. The solid curve denotes the initial relation between $m_*(j)$ and $J(j)$. The cross denotes the location of $m_*(j_{\mathrm{ISCO:max}})$ and $J(j_{\mathrm{ISCO:max}})$, which are the predicted final values of the mass and the angular momentum of a black hole.

lutionary track of the rest-mass and the angular momentum enclosed inside the apparent horizon. These results confirm the prediction (III) of the previous section. This conclusion is quite natural, in particular, in the present case because we initially reduce the pressure by a significant factor to quickly form a disklike structure, for which fluid elements of the same value of a cylindrical radius have almost the same value of j, and therefore, the initial distribution of $m_*(j)$ and $J(j)$ should determine the evolution of the system.

B. Results for $\Gamma = 2.0$

For comparison with the results of the moderately soft ($\Gamma = 1.5$) equation of state and for reconfirmation of the previous result by Stark and Piran [10], we also performed simulations for the rotating collapse adopting a stiff equation of state with $\Gamma = 2$. The simulations were performed with $N = 1000$ and $\Delta x = 0.005$ (in units of $G = c = K = 1$). To check the convergence, test simulations with a coarser grid resolution ($\Delta x = 0.0075$) were also performed, and we found that the numerical results depend very weakly on the grid resolution as long as $\Delta x \leq 0.0075$ and that the threshold for black hole formation is unchanged.

As in the case of $\Gamma = 1.5$, a black hole is formed even from the initial data sets with $q > 1$. In Figs. 13(a) and 13(b) we show the time evolution of the central density ρ_{*c} and the central value of the lapse function α_c for models listed in Table II. It is found that the rigidly rotating stars with $\Omega_0 \lesssim 0.67$ collapse to form a black hole. On the other hand, for the rigidly rotating stars with $\Omega_0 \gtrsim 0.68$, no black hole is formed. Therefore, the threshold value of q for the direct black hole formation is about ~ 1.2 for the rigidly rotating models with $\Gamma = 2$, which agrees approximately with that found by Stark and Piran [10] and is consistent with the result by Duez *et al.* [19]. For the critical model, the value of q_c is ≈ 0.92, close to unity. Since there is no reason to believe that the particularly large value of $q \sim 1.2$ should be the threshold for the black hole formation, we propose the quasilocal value of $q_c \approx 0.92 \sim 1$ as the threshold.

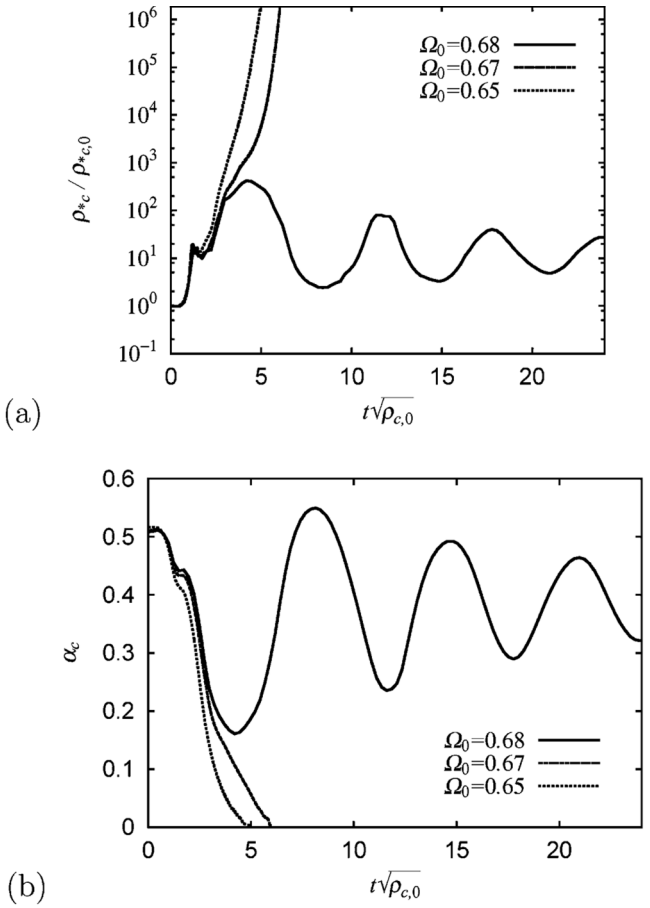

FIG. 13. Evolution of (a) the central density ρ_{*c} and (b) the central value of the lapse function α_c for $\Gamma = 2$. In both panels, the solid, dashed, and dotted curves denote the models of $\Omega_0 = 0.68$, 0.67, and 0.65, respectively.

A plausible reason why the critical value of q_c is somewhat smaller than unity may be as follows. First, note that the configuration of stars with stiffer equations of state is less centrally-condensed and more uniform, and thus, the collapse proceeds in a more coherent manner; i.e., the fluid elements collapse to a black hole rather simultaneously. Accordingly, the criterion for the black hole formation is unlikely to be determined only by the central properties of stars. Indeed, we find that ratio of the mass of the first seed apparent horizon to the total mass of the system for $\Gamma = 2.0$ is much larger than that for $\Gamma = 1.5$ case; $M_{\rm AH,seed}/M \sim 0.35$ at the critical value of q_c for $\Gamma = 2.0$, in contrast with that for $\Gamma = 1.5$, $M_{\rm AH,seed}/M \sim 0.1$. This indicates that for $\Gamma = 2$, not q_c but a value of $q(j)$ at a moderately large value of j (denoted as j_1) may determine the black hole formation (note that $q(j_1) < 1$). Since $q(j)$ is an increasing function of $m_*(j)$, $q(j_1)$ is larger than q_c and closer to unity. Therefore, the critical value in terms of q_c may well be smaller than unity for stiff equations of state.

Figure 14 shows the time evolution of $M_{\rm AH}$ for models with $\Gamma = 2.0$. It is found that the process of the black hole formation can also be divided into two phases: a phase in which a seed black hole is formed at the central region ($t \lesssim 5.6\rho_{c,0}^{-1/2}$) and the other phase in which the seed black hole grows as the ambient fluid falls into it ($t \gtrsim 5.6\rho_{c,0}^{-1/2}$).

Before closing this section, let us explain the reason that $q \approx 1$ has been believed as the threshold value for the black hole formation in the number of previous works. Stark and Piran [10] and Duez *et al.* [19] adopted only a *stiff* ($\Gamma = 2$) equation of state. As described above, such stars have rather uniform density distribution and the collapse proceeds fairly simultaneously for all the fluid elements. Furthermore, the distribution of $q(j)$ as a function of $m_*(j)$ with stiff equations of state is rather uniform. Indeed, for the rigidly rotating case with $\Gamma = 2.0$, q/q_c is $\sim$1.25 in contrast with the $\Gamma = 1.5$ cases for which $q/q_c \sim 2$ [compare Fig. 5 and Fig. 3(a)] for rigidly rotating models). These two facts imply that $q \approx 1$ may be an approximate threshold value for predicting no black hole formation in the case of $\Gamma = 2$. Nakamura and his collaborators performed simulation for *highly differentially rotating* stars [8,9]. The higher the degree of differential rotation becomes, the flatter the distribution of $q(j)$ is, as indicated in Fig. 4. As a result, the ratio q/q_c approaches unity. In their initial data, the degree of differential rotation is very high, and hence, q/q_c would be $\sim$1. This is the reason that the value $q \approx 1$ was regarded as the threshold of black hole formation. Abrahams *et al.* [11] performed simulations for toroidal star clusters. Having a toroidal configuration implies that they are rotating with a high degree of differential rotation. Again, $q_c \sim q$ for such systems, and hence, the global parameter q may be used as the threshold.

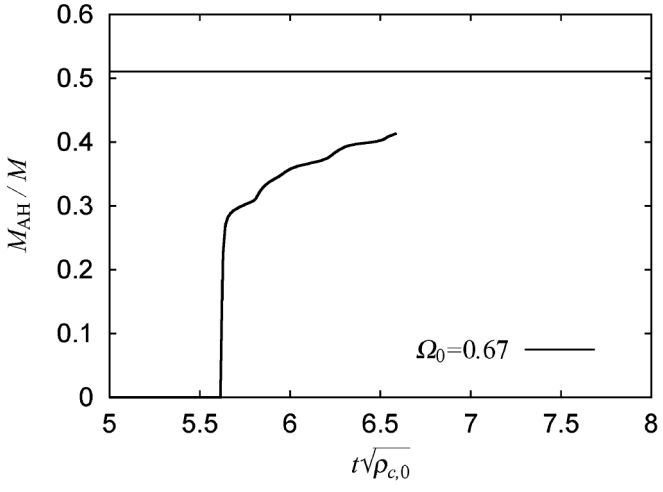

FIG. 14. Evolution of the apparent horizon mass $M_{\rm AH}$ for the rigidly rotating models with $\Gamma = 2.0$ and $\Omega_0 = 0.67$. The horizontal line of $M_{\rm AH} \approx 0.51M$ is $M_{\rm irr}$ in this case.

V. SUMMARY

We have reported new results about the black hole formation in the collapse of rapidly rotating stars with $q > 1$ and with moderately soft ($\Gamma = 1.5$) and stiff ($\Gamma = 2.0$) equations of state, analyzing initial conditions and performing axisymmetric simulations in full general relativity.

The initial conditions were given, following Stark and Piran [10]; we first gave marginally stable spherical polytropes with $\Gamma = 1.5$ or $\Gamma = 2.0$ and then artificially added an angular momentum and significantly deplete internal energy and pressure. Using the same analysis carried out in [7], we predicted that (I) the inner region in which $q_c \lesssim 1$ will collapse first to form a seed black hole even if the global value of q is much larger than unity; (II) the formed seed black hole will subsequently grow as the ambient fluid accretes onto it; (III) the evolution of the relation between the rest-mass and the angular momentum enclosed inside the growing black hole will agree approximately with the initial relation between $m_*(j)$ and $J(j)$; (IV) the final outcome of the dynamical collapse of sufficiently massive stars with $q > 1$ and $q_c < 1$ will be a black hole surrounded by an appreciable disk.

To confirm these predictions, we performed fully general relativistic hydrodynamic simulations using a high-resolution shock-capturing scheme with the Γ-law equations of state. As a result of numerical simulations, we confirmed the predictions (I), (II), and (III). From these results, we conclude that the previous criterion for black hole formation (i.e., no black hole is formed for $q \gtrsim 1$) is not always valid, in particular, for soft equations of state with $\Gamma \lesssim 1.5$. The universal criterion for no black hole formation is likely to be the condition $q_c \gtrsim 1$.

Previous works have suggested that $q \approx 1$ is the threshold value for the black hole formation. We have illustrated that this is approximately the case for $\Gamma = 2$. (This will be also the case for $\Gamma \geq 2$ since for such large values of Γ, $q/q_c \leq 1.25$.) However, this is not always the case for $\Gamma = 1.5$. The main reason is that stars with such soft equations of state have a centrally-concentrated density distribution. This results in the fact that the ratio q/q_c becomes ~ 2 for the rigidly rotating case with $\Gamma = 1.5$. This implies that even if q is much larger than unity, q_c can be much smaller than unity, and, namely, the central region of the star does not rotate so rapidly that the central region can form a black hole after collapse. For $\Gamma \leq 1.5$ and for the rigidly rotating case, $q/q_c \gtrsim 2$, and hence, predicting no black hole formation in terms of q becomes even worse. For $1.5 < \Gamma < 2$, we have not performed a simulation, and it is not clear whether $q = 1$ may be used as an approximate threshold. However, in this case, we know that $1.25 < q/q_c < 2$ for the rigidly rotating case, and therefore, q will also not be a very good parameter.

Numerical results suggest that prediction (IV) would be valid. To confirm it, however, it is necessary to perform a longterm simulation until the growth of black hole evolution terminates, which cannot be done at present. To perform such a long run, an excision technique will be required, but there is no good technique to follow the collapse with soft equations of state. Developing a robust excision technique that can be used for a wide variety of problems is one of the important issues in the field of numerical relativity.

Associated with the prediction (II), we have found that the process of black hole formation is divided into two phases: the first is the black hole formation phase in which the seed black hole is formed, and the other is the accretion phase in which a large amount of the ambient fluid elements are swallowed into the formed seed black hole. During the accretion phase, the system is composed of a black hole and the surrounding massive disk accreting onto the central black hole. The final state will be a rapidly rotating black hole surrounded by massive disks.

In the present paper, we have focused on clarifying the criterion of black hole formation analyzing simple toy models. To obtain a scientific result that can be compared with observational data such as gravitational waves, however, simulations with realistic initial conditions and realistic equations of state are necessary. The rapidly rotating black hole will be formed after rapidly rotating massive stellar core collapse and pair-unstable collapse, if the value of q_c for progenitors is smaller than unity at the onset of collapse. Formation of rapidly rotating black holes of $q_{\rm BH} \lesssim 1$ and accretion of the large mass onto such rapidly rotating black holes are likely to be strong burst sources of gravitational waves for the laser interferometric detectors. Thus, performing realistic numerical simulations of black hole formation is an important subject for predicting the gravitational waveforms. We plan to attack these computations in a fully general relativistic manner extending previous works [38,44].

For $q_c > 1$, the black hole will not be formed promptly. In such case, the collapse leads to formation of the self-gravitating disk or torus. They will be subsequently unstable against nonaxisymmetric deformation [19,28]. After the nonaxisymmetric instabilities turn on, the angular momentum will be transported from the inner region to the outer region, decreasing the value of $q(j)$ around the inner region below unity. As a result, the seed black hole may be formed. To follow these processes, it is necessary to perform a numerical simulation without assuming the axial symmetry. During the collapse, the typical length scale may change by a factor of 10^4 from $R/M \sim 10^4$ to 1. To follow the collapse by numerical simulation, very large computational resources will be necessary and, thus, the simulation for this phenomenon will be one of the computational challenges in the field of numerical relativity.

ACKNOWLEDGMENTS

Numerical computations were performed on the FACOM VPP5000 machine in the data processing center of National Astronomical Observatory of Japan and on the NEC SX6 machine in the data processing center of ISAS in JAXA. This work is in part supported by Japanese Monbu-Kagakusho Grants (No. 14047207, No. 15037204, No. 15740142, and No. 16029202).

[1] R. Penrose, Riv. Nuovo cimento **1**, 252 (1969).
[2] W. Israel, Phys. Rev. **164**, 1776 (1967).
[3] B. Carter, Phys. Rev. Lett. **26**, 331 (1971).
[4] D. C. Robinson, Phys. Rev. Lett. **34**, 905 (1975).
[5] S.W. Hawking and G. F. R. Ellis, *The Large Scale Structure of Space-time* (Cambridge University Press, Cambridge, 1973).
[6] R. M. Wald, *General Relativity* (University of Chicago Press, Chicago, 1984).
[7] M. Shibata, Astrophys. J. **605**, 350 (2004).
[8] T. Nakamura, Prog. Theor. Phys. **65**, 1876 (1981); **70**, 1144 (1983).
[9] T. Nakamura, K. Oohara, and Y. Kojima, Prog. Theor. Phys. Suppl. **90**, 1 (1987).

[10] R. F. Stark and T. Piran, Phys. Rev. Lett. **55**, 891 (1985); T. Piran and R. F. Stark in *Dynamical Spacetimes and Numerical Relativity*, edited by J. M. Centrella (Cambridge University Press, Cambridge, 1986).
[11] A. M. Abrahams, G. B. Cook, S. L. Shapiro, and S. A. Teukolsky, Phys. Rev. D **49**, 5153 (1994).
[12] M. Shibata, Prog. Theor. Phys. **104**, 325 (2000).
[13] M. Shibata, Astrophys. J. **595**, 992 (2003).
[14] M. Shibata and S. L. Shapiro, Astrophys. J. **572**, L39 (2002).
[15] K. Maeda, M. Sasaki, T. Nakamura, and S. Miyama, Prog. Theor. Phys. **63**, 719 (1980).
[16] J. M. Bardeen and T. Piran, Phys. Rep. **96**, 205 (1983).
[17] T.W. Baumgarte and S. L. Shapiro, Astrophys. J. **526**, 941 (1999).
[18] M. Shibata, T.W. Baumgarte, and S. L. Shapiro, Phys. Rev. D **61**, 044012 (2000).
[19] M. D. Duez, S. L. Shapiro, and H.-J. Yo, gr-qc/0401076.
[20] L. Baiotti, I. Hawke, P. J. Montero, F. Löffler, L. Rezzolla, N. Stergioulas, J. A. Font, and E. Seidel, gr-qc/0403029.
[21] M. D. Duez, Y. T. Liu, S. L. Shapiro, and B. C. Stephens, astro-ph/0402502.
[22] W. G. Unruh, (unpublished); J. Thornburg, Classical Quantum Gravity **4**, 1119 (1987).
[23] M. Alcubierre and B. Brügmann, Phys. Rev. D **63**, 104006 (2001).
[24] M. Shibata, Phys. Rev. D **67**, 024033 (2003).
[25] J. A. Font, Living Rev. Relativity **6**, 4 (2003); F. Banyuls, J. A. Font, J.-Ma. Ibáñez, J. M. Marti, and J. A. Miralles, Astrophys. J. **476**, 221 (1997).
[26] M. Shibata and T. Nakamura, Phys. Rev. D **52**, 5428 (1995).
[27] M. Shibata, Prog. Theor. Phys. **101**, 1199 (1999); Phys. Rev. D **60**, 104052 (1999).
[28] M. Shibata, T.W. Baumgarte, and S. L. Shapiro, Astrophys. J. **542**, 453 (2000).
[29] M. Shibata and K. Uryū, Phys. Rev. D **61**, 064001 (2000); Prog. Theor. Phys. **107**, 265 (2002).
[30] M. Shibata, K. Taniguchi, and K. Uryū, Phys. Rev. D **68**, 084020 (2003).
[31] M. Alcubierre, S. Brandt, B. Brügmann, D. Holz, E. Seidel, R. Takahashi, and J. Thornburg, Int. J. Mod. Phys. D **10**, 273 (2001).
[32] M. Alcubierre, B. Brügmann, D. Pollney, E. Seidel, and R. Takahashi, Phys. Rev. D **64**, 061501 (2001); L. Lindblom and M. A. Scheel, Phys. Rev. D **67**, 124005 (2003).
[33] M. Shibata, Phys. Rev. D **55**, 2002 (1997).
[34] J.. York, Jr. and T. Piran, in *Spacetime and Geometry: The Alfled Schild Lectures*, edited by R. A. Matzner and L. C. Shepley (University of Texas Press,, Austin, 1982).
[35] S. L. Shapiro and S. A. Teukolsky, *Black Holes, White Dwarfs, and Neutron Stars* (John Wiley & Sons, New York, 1983).
[36] J. M. Bardeen, W. H. Press, and S. A. Teukolsky, Astrophys. J. **178**, 347 (1972).
[37] V. P. Frolov and I. D. Novikov, *Black Hole Physics* (Kluwer Academic Publishers, Dordrecht, 1998).
[38] M. Shibata and Y. Sekiguchi, Phys. Rev. D **68**, 104020 (2003).
[39] R. F. Stark and T. Piran, Comput. Phys. Rep. **5**, 221 (1987).
[40] M. Shibata and Y. Sekiguchi, (unpublished).
[41] H.-J. Yo, T.W. Baumgarte, and S. L. Shapiro, Phys. Rev. D **64**, 124011 (2001); H.-J. Yo, T.W. Baumgarte, and S. L. Shapiro, Phys. Rev. D **66**, 084026 (2002).
[42] D. Shoemaker, K. S. Smith, U. Sperhake, P. Laguna, E. Schnetter, and D. Fiske, Classical Quantum Gravity **20**, 3729 (2003).
[43] E. Schnetter, S. H. Hawley, and I. Hawke, Classical Quantum Gravity **21**, 1465 (2004).
[44] M. Shibata and Y. Sekiguchi, Phys. Rev. D **69**, 084024 (2004).